Data-driven algorithms for nonautonomous Koopman operator

Senka Maćešić

(joint work with Nelida Črnjarić-Žic and Igor Mezić)

Operator Theoretic Methods in Dynamic Data Analysis and Control

February 11-15 2019

Process and the nonautonomous flow

Let $\mathbb{T}$ be an additive semigroup (or group) with a metric space structure ($\mathbb{Z}$, $\mathbb{Z}_0^+$, $\mathbb{R}$, or $\mathbb{R}_0^+$). We call $\mathbb{T}$ the time set.
Let (X, d_X) be a metric state space and $\mathbb{T}$ a time set. Let $\mathbf{S} : \mathbb{T} \times \mathbb{T} \times X \to X$ be a continuous mapping such that the two-parameter family $\mathbf{S}^{t,t_0} = \mathbf{S}(t, t_0, \cdot)$, $t, t_0 \in \mathbb{T}$ satisfies the cocycle property

$$\mathbf{S}^{t_0,t_0} = id_X \quad \text{and} \quad \mathbf{S}^{t+s,t_0} = \mathbf{S}^{t+s,t} \circ \mathbf{S}^{t,t_0} \quad \text{for} \quad t_0 \leq t \leq t+s, \ t_0, t, s \in \mathbb{T}. \tag{1}$$

The mapping $\mathbf{S}$ is called the process and the two-parameter family $\mathbf{S}^{t,t_0}$ is called the nonautonomous flow.

Consider the case of a nonautonomous differential equation

$$\dot{\mathbf{x}} = \mathbf{F}(t, \mathbf{x}) \tag{2}$$

on $X = \mathbb{R}^d$. Assume $\mathbf{x} = \mathbf{x}(t, t_0, \mathbf{x}_0)$ is the solution of (2) satisfying the condition $\mathbf{x}(t_0, t_0, \mathbf{x}_0) = \mathbf{x}_0$. Then, equation (2) generates the nonautonomous flow $\mathbf{S}^{t,t_0}(\mathbf{x}_0) = \mathbf{x}(t, t_0, \mathbf{x}_0)$.

Process formulation of the nonautonomous Koopman operator

Definition

Let $\mathbf{S}^{t,t_0}$ be a nonautonomous flow and U^{t,t_0} an operator family defined on the space of observables $f : X \to \mathbb{C}$ by

$$U^{t,t_0} f = f \circ \mathbf{S}^{t,t_0}. \tag{3}$$

Then U^{t,t_0} is called the nonautonomous Koopman operator family. If $\lambda^{t,t_0} \in \mathbb{C}$ and observable $\phi_{\lambda^{t,t_0}} : X \to \mathbb{C}$ are such that

$$U^{t,t_0} \phi_{\lambda^{t,t_0}} = e^{\lambda^{t,t_0}} \phi_{\lambda^{t,t_0}}, \tag{4}$$

they are called the nonautonomous Koopman operator eigenvalue and eigenfunction.

Koopman mode decomposition for the linear nonautonomous dynamical system (process formulation)

Proposition

If $\mathbf{A} : \mathbb{R} \to \mathbb{R}^{d\times d}$ *is continuous, then the linear nonautonomous differential equation*

$$\dot{\mathbf{x}} = \mathbf{A}(t)\mathbf{x} \tag{5}$$

generates a linear nonautonomous flow $\mathbf{S}^{t,t_0} : \mathbb{R}^d \to \mathbb{R}^d$ *satisfying*

$$\mathbf{S}^{t,t_0}\mathbf{x} = \mathbf{x} + \int_{t_0}^{t} \mathbf{A}(\tau)\mathbf{S}^{\tau,t_0}\mathbf{x}\, d\tau. \tag{6}$$

If $\mathbf{S}^{t,t_0}$ *is diagonalizable, with simple eigenvalues* $\mu_j^{t,t_0} = e^{\lambda_j^{t,t_0}}$ *and left and right eigenvectors* $\mathbf{w}_j^{t,t_0}$, $\mathbf{v}_j^{t,t_0}$, $j = 1,\ldots,d$, *then* $\phi_j^{t,t_0}(\mathbf{x}) = \langle \mathbf{x}, \mathbf{w}_j^{t,t_0}\rangle$, $j = 1,\ldots,d$, *are the eigenfunctions of the nonautonomous Koopman operator* U^{t,t_0} *with the corresponding eigenvalues* λ_j^{t,t_0}, $j = 1,\ldots,d$. *Furthermore,* $\mathbf{v}_j^{t,t_0}$, $j = 1,\ldots,d$ *are the Koopman modes of the full-state observable and the following expansion is valid*

$$U^{t,t_0}\mathbf{x}_0 = \sum_{j=1}^{d} \langle \mathbf{x}_0, \mathbf{w}_j^{t,t_0}\rangle e^{\lambda_j^{t,t_0}} \mathbf{v}_j^{t,t_0}. \tag{7}$$

Moving stencil approach (1)

Suppose that for some linear non-autonomous system (5) we have a sequence of snapshots of the full-state observable

$$\mathbf{x}_k = \mathbf{x}(t_k), k = 0, 1, ... \tag{8}$$

where $t_k = k\Delta t$, $k = 0, 1, ...$ Our goal is to compute approximations of the principal eigenvalues and principal eigenfunctions of the Koopman operators U^{t_k, t_0}, $k = 0, 1, ...$ from these snapshots.
This task can be reduced to the computation of $\mathbf{S}^{t_k, t_0}$, $k = 0, 1, ...$ Since it satisfies the cocycle property, we get

$$\mathbf{S}^{t_k, t_0} = \mathbf{S}^{t_k, t_{k-1}} \mathbf{S}^{t_{k-1}, t_0}, k = 1, 2, ... \tag{9}$$

This gives us the possibility to further reduce the problem to an approximate evaluation of local $\mathbf{S}^{t_k, t_{k-1}}$, $k = 1, 2, ...$
In order to do this, let us look at the local stencil of snapshots

$$\mathbf{x}_{k-1}, \mathbf{x}_k, ..., \mathbf{x}_{k+s-1} \tag{10}$$

where s is fixed over the computational domain. We use this forward-positioned stencil for technical reasons, since otherwise there would be no data for the first local $\mathbf{S}^{t_1, t_0}$.

Moving stencil approach (2)

To this local stencil (10) we can apply any of the Krylov subspace methods and obtain a matrix $\mathbf{M}_{k,k-1}$ such that

$$\mathbf{x}_{k+j} \approx \mathbf{M}_{k,k-1}\mathbf{x}_{k+j-1}, j = 0, 1, ..., s-1 \tag{11}$$

The approximation is obtained by the projection of $\mathbf{x}_{k+s-1}$ to the Krylov subspace spanned by $\mathbf{x}_{k-1}, \mathbf{x}_k, ..., \mathbf{x}_{k+s-2}$

$$c_0\mathbf{x}_{k-1} + c_1\mathbf{x}_k + \cdots c_{s-1}\mathbf{x}_{k+s-2} = \mathbf{x}_{k+s-1} + \mathbf{r}_k \tag{12}$$

under the condition that

$$\mathbf{r}_k \perp \mathbf{x}_{k-1}, \mathbf{x}_k, ..., \mathbf{x}_{k+s-2}. \tag{13}$$

The matrix representation of the projection operator in basis $\mathbf{x}_{k-1}, \mathbf{x}_k, ..., \mathbf{x}_{k+s-2}$ is given by the companion matrix

$$\mathbf{C} = \begin{pmatrix} 0 & 0 & \cdots & 0 & c_0 \\ 1 & 0 & \cdots & 0 & c_1 \\ 0 & 1 & \cdots & 0 & c_2 \\ \vdots & \ddots & \ddots & \vdots & \vdots \\ 0 & 0 & \cdots & 1 & c_{s-1} \end{pmatrix}. \tag{14}$$

Moving stencil approach (3)

The condition (13) guaranties that the projection error

$$\|\mathbf{r}_k\|_2 = \|\mathbf{x}_{k+s-1} - (c_0\mathbf{x}_{k-1} + c_1\mathbf{x}_k + \cdots c_{s-1}\mathbf{x}_{k+s-2})\|_2 \tag{15}$$

is minimal. Observe that the companion matrix (14) is a representation of a finite-dimensional approximation of the Koopman operator $U^{t_k,t_{k-1}}$ relative to the Krylov basis, while the matrix $\mathbf{M}_{k,k-1}$ is a representation of the same approximation, but relative to the basis in which (5) is written. After we find $\mathbf{M}_{k,k-1}$, $k = 1, 2, ...$, we can construct the approximate fundamental matrix family

$$\mathbf{M}_{0,0} = \mathbf{I},\ \mathbf{M}_{k,0} = \mathbf{M}_{k,k-1}\mathbf{M}_{k-1,0}, \quad k = 1, 2, ..., \tag{16}$$

We can use these matrices for the computation of the Koopman eigenvalue approximations and also for the reconstruction of the original data

$$\tilde{\mathbf{x}}_k = \mathbf{M}_{k,0}\mathbf{x}_0, \quad k = 1, 2, ..., \tag{17}$$

which is the same as the Koopman mode decomposition (7) done with eigenvalues and eigenvectors of the approximate fundamental matrix $\mathbf{M}_{k,0}$, $k = 1, 2, ...$ We will call this approach the moving stencil approach. In order to possibly capture all principal eigenvalues, we use $s = n$.

Example of a nonlinear nonautonomous dynamical system (1)

We consider the nonlinear dynamical system

$$\begin{aligned} \dot{x}_1 &= \sigma_1 x_1 \\ \dot{x}_2 &= \sigma_2 (x_2 - x_1^2). \end{aligned} \tag{18}$$

If $\sigma_1, \sigma_2 \in \mathbb{R}$, the system is autonomous, and two of the autonomous Koopman operator eigenvalues and eigenfunctions are

$$\lambda_1 = \sigma_1, u_1(\mathbf{x}) = x_1 \tag{19}$$

and

$$\lambda_2 = \sigma_2, u_2(\mathbf{x}) = x_2 - \frac{\sigma_2}{\sigma_2 - 2\sigma_1} x_1^2. \tag{20}$$

If we have snapshots from that nonlinear autonomous dynamical system we can try to compute the eigenvalues and eigenfunctions (19)-(20) by applying the moving stencils approach. If we use full-state observables, some error occurs due to nonlinearity (1). It is easy to see that in this example, the error depends on the initial condition used. To obtain accurate values with the moving stencils approach, it is enough to use observables

$$y_1 = x_1, y_2 = x_2, y_3 = x_1^2 \tag{21}$$

instead of the full-state observables.
These observables are equivalent with the Carleman linearization of (18)

$$\dot{\mathbf{y}} = \mathbf{A}\mathbf{y}, \tag{22}$$

Example of a nonlinear nonautonomous dynamical system (2)

where

$$\mathbf{A} = \begin{pmatrix} \sigma_1 & 0 & 0 \\ 0 & \sigma_2 & -\sigma_2 \\ 0 & 0 & 2\sigma_1 \end{pmatrix}. \tag{23}$$

Let us emphasize that in the general case of a non-linear dynamical system, the Carleman linearization will lead to a linear finite-dimensional approximation of the original dynamical system. Then, the principal Koopman operator eigenvalues of the linearized approximation, even if computed analytically, will be just approximations of a finite subset of the Koopman operator eigenvalues of the original system. Related principal Koopman operator eigenfunctions of the linearized approximation will be linear in the new state vector. They will form a finite subset of Koopman operator eigenfunctions of the original non-linear system and they will be non-linear relative to the original full-state vector.
For this linearized system, an additional eigenvalue-eigenfunction pair appears

$$\lambda_3 = 2\sigma_1, u_3(\mathbf{x}) = x_1^2. \tag{24}$$

Krylov subspace methods would typically correctly identify (19)-(20) from the snapshots of observables 21 (1 (a) and (b)), and with the moving stencils approach we obtain time-dependent variants, which in this autonomous case are reduced to $\sigma_i(t - t_0)$, $i = 1, 2$ (1 (c) and (d)).

Example of a nonlinear nonautonomous dynamical system (3)

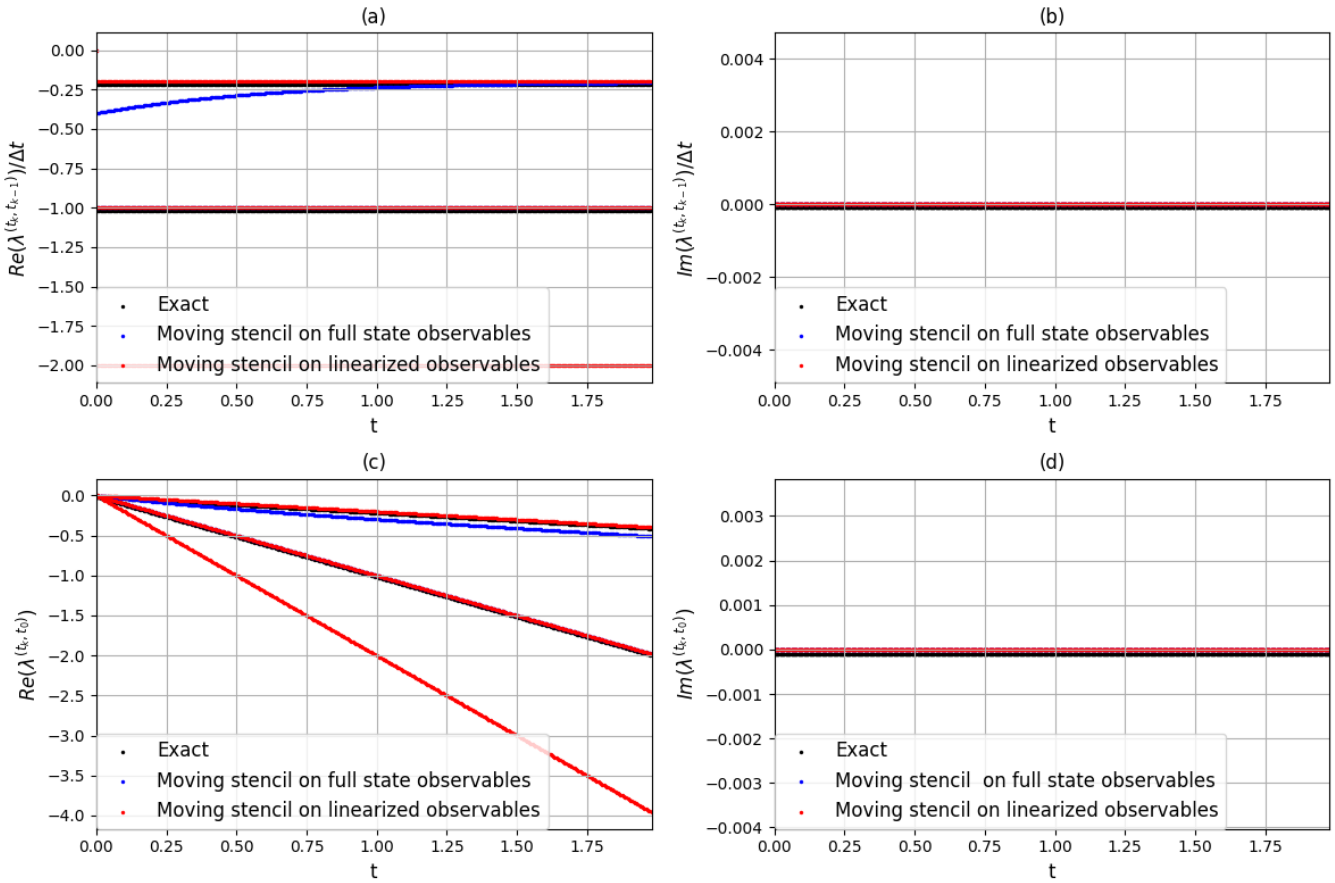

Figure: Dynamical system (18), autonomous case and initial condition $(-1, 1)$: (a) and (b) dynamical system matrix eigenvalues, (c) and (d) Koopman operator eigenvalues (Exact values are offset to improve visibility.)

Example of a nonlinear nonautonomous dynamical system (4)

Now, let us consider the non-autonomous case by introducing time dependency $\sigma_1 = \sigma_1(t)$, $\sigma_2 = \sigma_2(t)$ in (18). In particular, we take

$$\sigma_i(t) = \sigma_{i,0} + A_i \cos(\omega_i t) + B_i \sin(\omega_i t), i = 1, 2 \tag{25}$$

with $\sigma_{1,0} = -1$, $\sigma_{2,0} = -0.05$, $A_1 = B_1 = 0.1$, $\omega_1 = 8$, and $A_2 = B_2 = 0$. We can also proceed with the Carleman linearization (21)-(23), but now, obviously, $\mathbf{A} = \mathbf{A}(t)$ in (23). The moving stencils approach gives good results if it is used for data reconstruction (17) ((2) (a) and (c)). On the other hand, as we can see in (2) (b) and (d), the moving stencils approach will give highly incorrect eigenvalues. Note that this is happening on the observables which linearize the system and completely solve all issues in the autonomous case. In the non-autonomous case, the same choice of observables is not good enough.

So, we must take a deeper look into the nature of this issue specific to non-autonomous Koopman operator family eigenvalues. Let us start with an analysis of a similar error that appears when dynamical system matrix has pairs of complex conjugate eigenvalues.

Example of a nonlinear nonautonomous dynamical system (5)

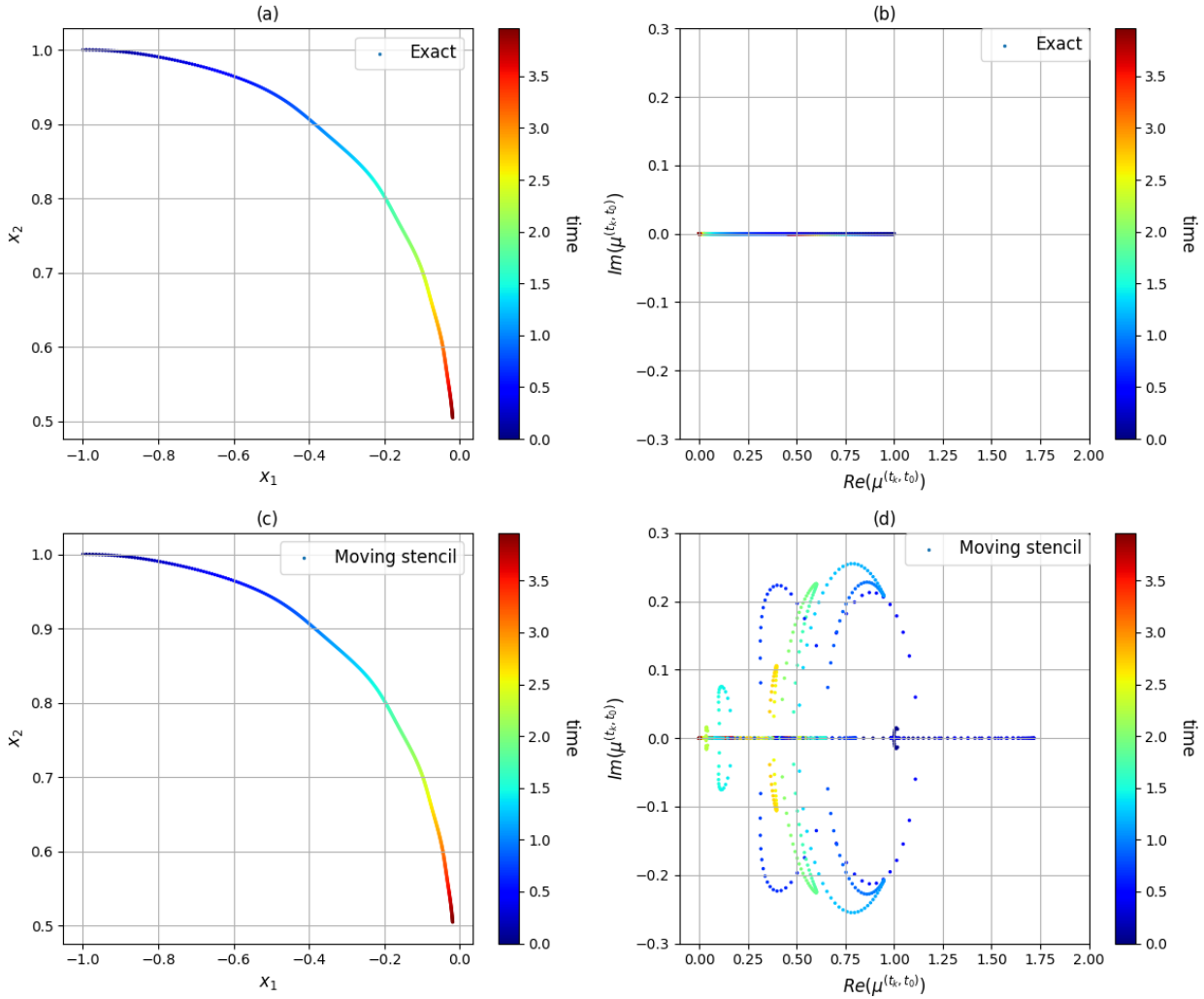

Figure: Dynamical system (18), linearized non-autonomous case: (a) and (c) the solution for the initial condition (-1,1); (b) and (d) the fundamental matrix eigenvalues.

Error of the moving stencil approach (1)

Theorem

Consider the dynamical system (5) with diagonalizable matrix $\mathbf{A}(t)$ *in the canonical form*

$$\mathbf{A}(t) = \begin{pmatrix} \mathbf{A}_{\lambda_1}(t) & \mathbf{0} & \dots & \mathbf{0} \\ \mathbf{0} & \mathbf{A}_{\lambda_2}(t) & \dots & \mathbf{0} \\ \vdots & \vdots & \ddots & \vdots \\ \mathbf{0} & \mathbf{0} & \dots & \mathbf{A}_{\lambda_m}(t) \end{pmatrix} \tag{26}$$

where

$$\mathbf{A}_{\lambda_j}(t) = \begin{pmatrix} \sigma_j(t) & \omega_j(t) \\ -\omega_j(t) & \sigma_j(t) \end{pmatrix} \tag{27}$$

is a Jordan block in the real form, belonging to the complex conjugate pair of eigenvalues $\lambda_j(t) = \sigma_j(t) + i\omega_j(t)$, $\bar{\lambda}_j(t) = \sigma_j(t) - i\omega_j(t)$, *with* $\omega_j, \sigma_j \in C^2([t_0, \infty))$, $\omega_j \neq 0$, *for all* $j = 1, ..., m$, $n = 2m$.
If $\tilde{\lambda}_j$, $j = 1, ..., m$ *are the eigenvalues obtained with the Krylov subspace method, then*

$$\tilde{\lambda}_j(t) = \lambda_j(t) + \frac{\dot{\omega}_j(t)}{2\omega_j(t)} - i\frac{\dot{\sigma}_j(t)}{\sqrt{\omega_j(t)^2 - \dot{\sigma}_j(t)} + \omega_j(t)} + \mathcal{O}(\Delta t) \tag{28}$$

for every $t \in [t_0, \infty)$, $j = 1, ..., m$.

Error of the moving stencil approach (2)

Theorem

Consider the dynamical system (5) with matrix $\mathbf{A}(t)$ *in the canonical form (26) where*

$$\mathbf{A}_{\lambda_j}(t) = \begin{pmatrix} \lambda_j(t) & 1 \\ 0 & \lambda_j(t) \end{pmatrix} \tag{29}$$

is a Jordan block $\mathbf{A}_{\lambda_j}(t)$*, belonging to the complex eigenvalue* $\lambda_j(t) = \sigma_j(t) + i\omega_j(t)$ *of multiplicity two, with* $\omega_j, \sigma_j \in C^2([t_0, \infty))$*,* $j = 1, ..., m$*,* $n = 2m$*.*
If $\tilde{\lambda}_j$*,* $j = 1, ..., m$ *are the eigenvalues obtained with the Krylov subspace method, then*

$$\tilde{\lambda}_j(t) = \left(\lambda_j(t) \pm \sqrt{\dot{\lambda}_j(t)}\right) + \mathcal{O}(\Delta t). \tag{30}$$

for every $t \in [t_0, \infty)$*,* $j = 1, ..., m$*.*

Error of the moving stencil approach (3)

Theorem

If $\tilde{\lambda}$ is the eigenvalue obtained with the Krylov subspace method applied to a vector observable $\mathbf{f} : X \to \mathbb{C}^N$ such that $\mathbf{f}(\mathbf{x}(t))$ is C^3, then

$$\tilde{\lambda} = \frac{\langle \dot{\mathbf{f}}_0, \mathbf{f}_0 \rangle}{\langle \mathbf{f}_0, \mathbf{f}_0 \rangle} + \mathcal{O}(\Delta t) \tag{31}$$

in the two-snapshots case, and

$$\tilde{\lambda} = \frac{\langle \ddot{\mathbf{f}}_0, \mathbf{f}_0 \rangle}{\langle \dot{\mathbf{f}}_0, \mathbf{f}_0 \rangle} + \mathcal{O}(\Delta t) \tag{32}$$

in the three-snapshots case.

Error of the moving stencil approach (4)

Consider the simplest case, when $\mathbf{f}$ is the full-state observable of a nonautonomous dynamical system that is linearized and diagonalized, i.e. $\mathbf{f}(t) = \mathbf{x}(t)$ such that

$$\dot{\mathbf{x}} = \Lambda(t)\mathbf{x}. \tag{33}$$

Then

$$\ddot{\mathbf{x}} = \left(\dot{\Lambda}(t) + \Lambda(t)^2\right)\mathbf{x}, \tag{34}$$

and Theorem 4 means that for the three-snapshots case Krylov subspace methods will give us the following approximation of eigenvalues

$$\tilde{\lambda} = \frac{\langle\left(\dot{\Lambda}(t_0) + \Lambda(t_0)^2\right)\mathbf{x}_0, \mathbf{x}_0\rangle}{\langle\Lambda(t_0)\mathbf{x}_0, \mathbf{x}_0\rangle} + \mathcal{O}(\Delta t). \tag{35}$$

Therefore, even with the right choice of the initial state $\mathbf{x}_0$ instead of obtaining one of the exact eigenvalues $\lambda(t_0)$ or at least an approximation that decreases with the decrese of the time step, we obtain

$$\tilde{\lambda} = \lambda(t_0) + \frac{\dot{\lambda}(t_0)}{\lambda(t_0)} + \mathcal{O}(\Delta t). \tag{36}$$

i.e., the error in the obtained approximation is proportional to the time derivative of that eigenvalue.

Algorithm 2 (that corrects the error)

Input: Sequence of snapshots $\mathbf{x}_k = \mathbf{x}(t_k)$, $k = 0, 1, ...$ from a non-linear non-autonomous dynamical system.

Output: Approximations of a finite set of Koopman operator eigenvalues λ_i^{t,t_0} and eigenfunctions $\phi_i^{t,t_0}(\cdot)$, $i = 1, ..., n$

1: Use linearization, conjugacy, or similar techniques to obtain a new set of observables $\mathbf{u} = (u_1, ..., u_m)^T$ for which we can take $s = 1$.
2: **for** $k = 0, 1, ...$ **do**
3: Apply the Standard DMD to the local stencil of two snapshots $\{u_i(t_{k-1}), u_i(t_k)\}$, separately for each $i = 1, ..., m$, and then determine $\tilde{\mathbf{M}}_{k,k-1}$.
4: Compute $\tilde{\mathbf{M}}_{k,0} = \tilde{\mathbf{M}}_{k,k-1}\tilde{\mathbf{M}}_{k-1,0}$.
5: Compute dynamical system matrix eigenvalues from $\tilde{\mathbf{M}}_{k,k-1}$ and Koopman operator eigenvalues from $\tilde{\mathbf{M}}_{k,0}$.
6: **end for**

Example of a nonlinear nonautonomous dynamical system (continued, 6)

Now we can return to our non-linear non-autonomous dynamical system (18). Observe that, in this case, the error is of the same nature as in Theorems 2 and 3 but is not covered by the statements in those theorems. Only if we apply Algorithm 2, in the sense that we find such observables for which stencil size can be reduced, the non-autonomous Koopman operator eigenvalues can be accurately computed. In this example, we can achieve this by using observables $\mathbf{u} = \begin{pmatrix} u_1 & u_2 \end{pmatrix}^T$ from (19)-(20). If we define such observables and proceed with Algorithm 2, we obtain excellent results (Fig.3).

Example of a nonlinear nonautonomous dynamical system (7)

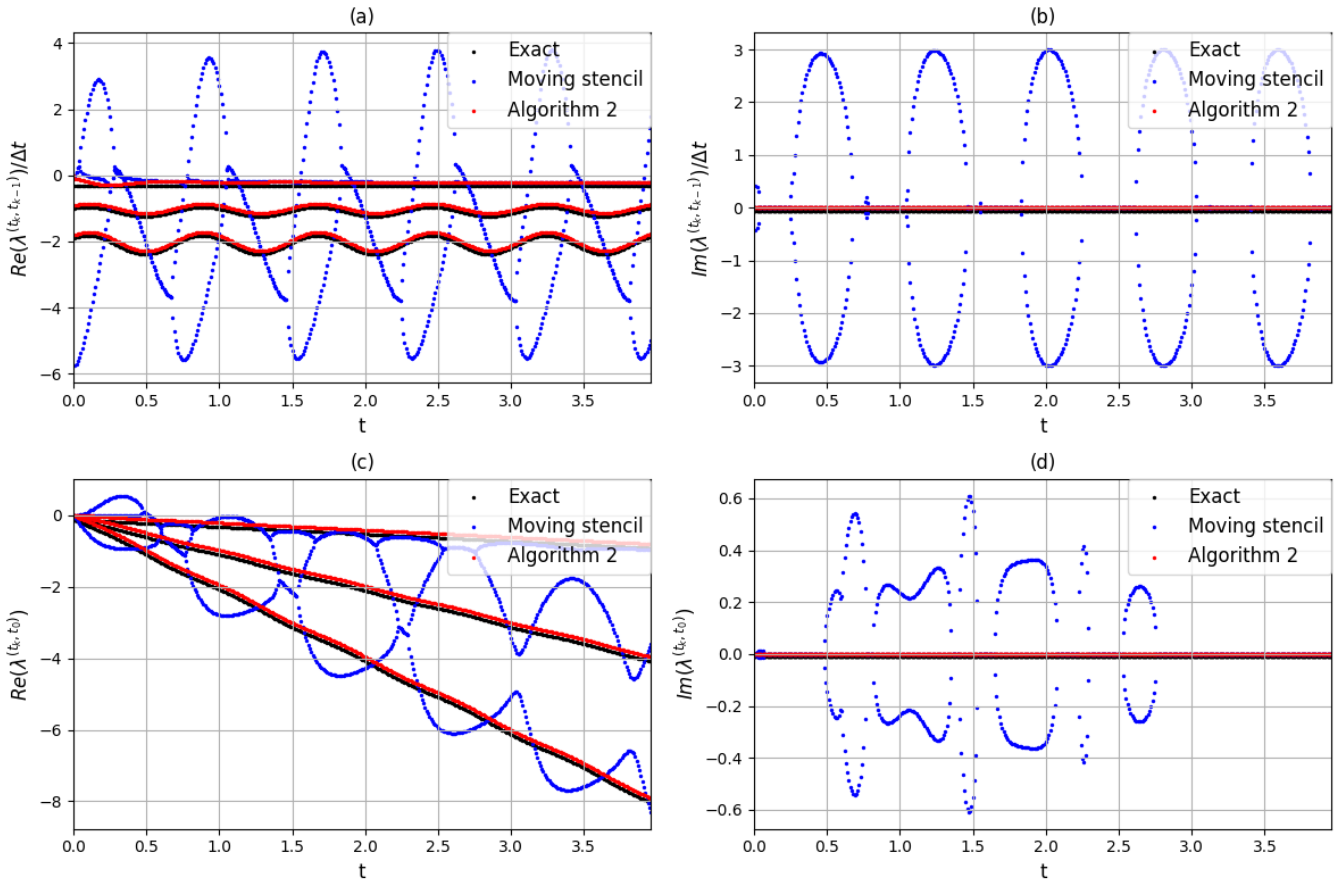

Figure: Dynamical system (18), linearized non-autonomous case: (a) and (b) dynamical system matrix eigenvalues, (c) and (d) Koopman operator eigenvalues (Exact values are offset to improve visibility.)

Example of a nonautonomous system with continuous frequency change and noise (1)

In this example, we consider an oscillator with a continuously changing frequency. The governing equations are (5) with the underlying matrix of the form (26)-(27) with only one Jordan block, where we additionally set $\sigma(t) = 0$ and

$$\omega(t) = \omega_0 + A_d \cos(\omega_d t) + B_d \sin(\omega_d t). \tag{37}$$

We can obtain the eigenvalues analytically using the fundamental matrix

$$\mathbf{S}_j^{t,t_0} = e^{\alpha_j(t,t_0)} \begin{pmatrix} \cos\beta_j(t,t_0) & \sin\beta_j(t,t_0) \\ -\sin\beta_j(t,t_0) & \cos\beta_j(t,t_0) \end{pmatrix}, \tag{38}$$

where $\alpha(t,t_0) = 0$ and

$$\beta(t,t_0) = \omega_0(t-t_0) + \frac{A_d}{\omega_d}\left(\sin(\omega_d t) - \sin(\omega_d t_0)\right) - \frac{B_d}{\omega_d}\left(\cos(\omega_d t) - \cos(\omega_d t_0)\right). \tag{39}$$

The computations are performed for $\omega_0 = 2$, $\omega_d = \pi$, and $A_d = 0.5$. We added relative uniform noise of order 10^{-4} to the data.

Example of a nonautonomous system with continuous frequency change and noise (2)

When computations are performed with any Krylov subspace method on moving stencils, the numerically evaluated real part of the eigenvalue of the underlying matrix displays a nonexistent time-dependency (Fig. 4(a)), while the imaginary parts of those eigenvalues are correct (Fig. 4(b)). As proven in Theorem 2, the numerical result for the imaginary part of the dynamical system matrix eigenvalues are correct because there is no time change in σ. Also, as proven in Theorem 2, numerical results for the real part of the dynamical system matrix eigenvalues are compromised by the error which is proportional to the time derivative of $\omega(t)$.
This error then propagates into the principal Koopman operator eigenvalue computations (Fig. 4 (c)-(d)). From those results it might be concluded that there is an amplitude change in the system and that even at some time moments frequencies stay at the value $\pm\pi$ (Fig. 4(d)), and then real parts of the principal eigenvalues split into two different values (Fig. 4(c)). All of this is completely erroneous.
The results obtained using Algorithm 2 are in accordance with the exact computations. In Fig. 4 (a) and (c), we see that the real parts of both the dynamical system matrix and the principal Koopman operator eigenvalues stay equal to zero at all times. Imaginary parts of dynamical system matrix eigenvalues (Fig. 4(b)) and the principal Koopman operator eigenvalues (Fig. 4(d)) computed with Algorithm 2 show the correct time-dependency.

Example of a nonautonomous system with continuous frequency change and noise (3)

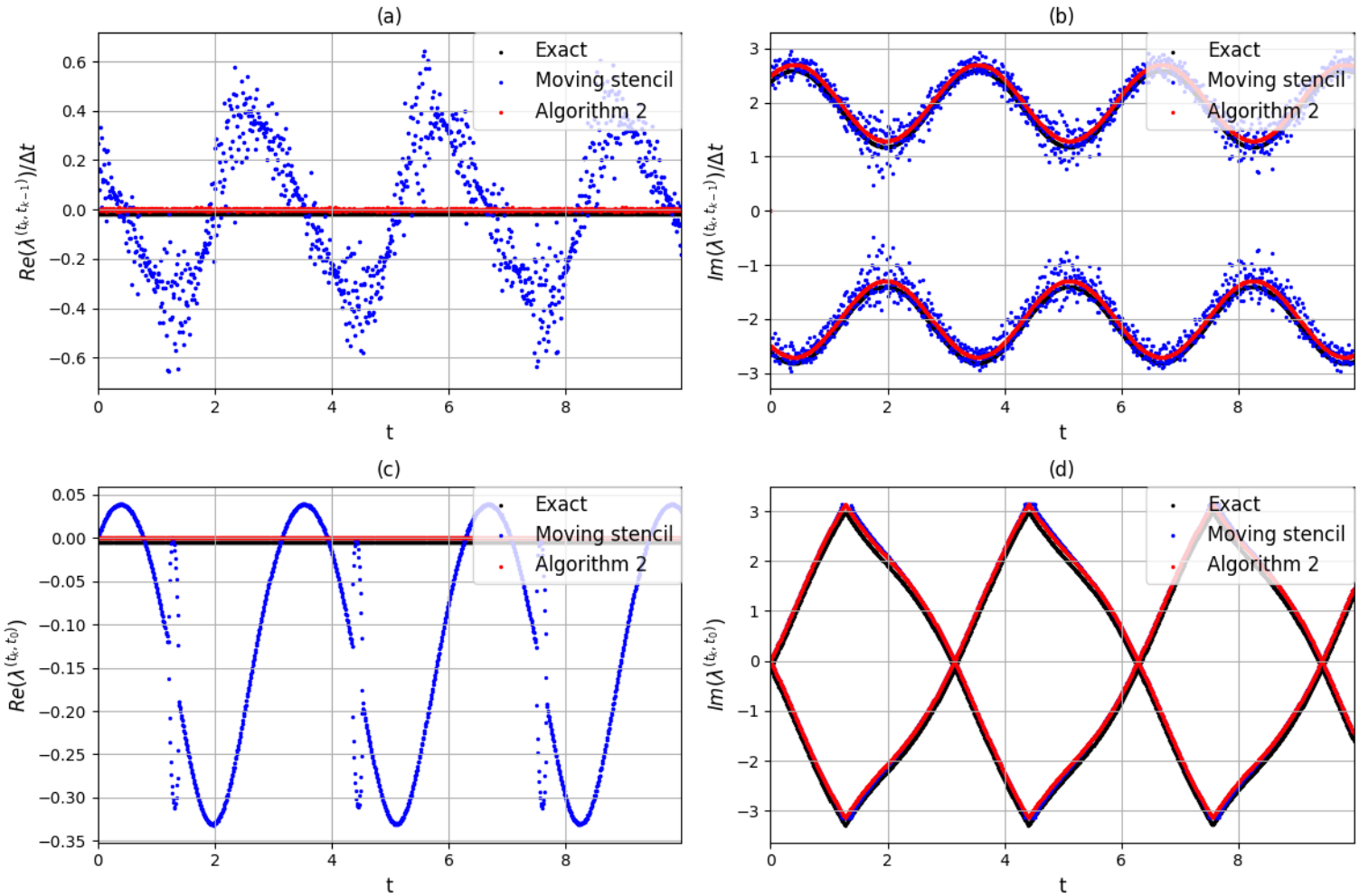

Figure: Dynamical system with continuous frequency change (37) and added relative uniform noise of order 10^{-4}: (a) and (b) dynamical system matrix eigenvalues, (c) and (d) principal Koopman operator eigenvalues (Exact values are computed without noise and offset to improve visibility.)

Skew product flow

Let (P, d_P) be a metric state space and $\mathbb{T}$ a time set. Let $\theta : \mathbb{T} \times P \to P$ be a continuous mapping such that family $\theta^t = \theta(t, \cdot)$, $t \in \mathbb{T}$ forms a group of bi-continuous mappings and satisfies the cocycle property

$$\theta^0 = id_P \quad \text{and} \quad \theta^{t+s} = \theta^s \circ \theta^t \quad \text{for} \quad t, s \in \mathbb{T}. \tag{40}$$

Let (X, d_X) be a metric state space and let $\mathbf{S} : \mathbb{T}_0^+ \times P \times X \to X$ be a continuous mapping such that the two-parameter family $\mathbf{S}^{t,\mathbf{p}} = \mathbf{S}(t, \mathbf{p}, \cdot)$, $t \in \mathbb{T}$, $\mathbf{p} \in P$ satisfies the cocycle property over θ^t

$$\mathbf{S}^{0,\mathbf{p}} = id_X \quad \text{and} \quad \mathbf{S}^{t+s,\mathbf{p}} = \mathbf{S}^{s,\theta^t(\mathbf{p})} \circ \mathbf{S}^{t,\mathbf{p}}, \quad \text{for} \quad t, s \in \mathbb{T}_0^+, \ \mathbf{p} \in P. \tag{41}$$

The mapping pair $(\theta, \mathbf{S})$ is called the nonautonomous dynamical system and θ its driving dynamical system. Furthermore, the mapping $\mathbf{S}_s : \mathbb{T}_0^+ \times P \times X \to P \times X$ defined by

$$\mathbf{S}_s(t, (\mathbf{p}, \mathbf{x})) = (\theta(t, \mathbf{p}), \mathbf{S}(t, \mathbf{p}, \mathbf{x})) \tag{42}$$

forms an autonomous semi-dynamical system on $P \times X$. The family $\mathbf{S}_s^t = \mathbf{S}_s(t, \cdot)$, $t \in \mathbb{T}$ is called the skew product flow associated with the nonautonomous dynamical system $(\theta, \mathbf{S})$.

Definition

Let $\mathbf{S}^{t,\mathbf{p}_0}$ be a nonautonomous flow and $U^{t,\mathbf{p}_0}$ an operator family defined on the space of observables, i.e., scalar valued functions $f : X \to \mathbb{C}$ by

$$U^{t,\mathbf{p}_0} f = f \circ \mathbf{S}^{t,\mathbf{p}_0}. \tag{43}$$

Then $U^{t,\mathbf{p}_0}$ is called the nonautonomous Koopman operator family. If $\lambda^{t,\mathbf{p}_0} \in \mathbb{C}$ and observable $\phi_{\lambda^{t,\mathbf{p}_0}} : X \to \mathbb{C}$ are such that

$$U^{t,\mathbf{p}_0} \phi_{\lambda^{t,\mathbf{p}_0}} = e^{\lambda^{t,\mathbf{p}_0}} \phi_{\lambda^{t,\mathbf{p}_0}}, \tag{44}$$

they are called the nonautonomous Koopman eigenvalue and eigenfunction.

Koopman mode decomposition for the linear nonautonomous dynamical system (skew product flow formulation)

Proposition

If $\mathbf{A} : \mathbb{R}^m \to \mathbb{R}^{d\times d}$ *is continuous, and* $\theta : \mathbb{R} \times \mathbb{R}^m \to \mathbb{R}^m$ *satisfies the conditions for the driving dynamical system, then linear nonautonomous differential equation*

$$\dot{\mathbf{x}} = \mathbf{A}(\theta(t, \mathbf{p}_0))\mathbf{x} \tag{45}$$

generates a linear nonautonomous flow $\mathbf{S}^{t,\mathbf{p}_0} : \mathbb{R}^d \to \mathbb{R}^d$ *satisfying*

$$\mathbf{S}^{t,\mathbf{p}_0}\mathbf{x} = \mathbf{x} + \int_0^t \mathbf{A}(\theta(\tau, \mathbf{p}_0))\mathbf{S}^{\tau,\mathbf{p}_0}\mathbf{x}\, d\tau. \tag{46}$$

If $\mathbf{S}^{t,\mathbf{p}_0}$ *is diagonalizable, with simple eigenvalues* $\mu_j^{t,\mathbf{p}_0} = e^{\lambda_j^{t,\mathbf{p}_0}}$ *and left and right eigenvectors* $\mathbf{w}_j^{t,\mathbf{p}_0}$, $\mathbf{v}_j^{t,\mathbf{p}_0}$, $j = 1, \ldots, d$, *then* $\phi_j^{t,\mathbf{p}_0}(\mathbf{x}) = \langle \mathbf{x}, \mathbf{w}_j^{t,\mathbf{p}_0} \rangle$, $j = 1, \ldots, d$,*are the eigenfunctions of the nonautonomous Koopman operator* $U^{t,\mathbf{p}_0}$ *with the corresponding eigenvalues* $\lambda_j^{t,\mathbf{p}_0}$, $j = 1, \ldots, d$. *Furthermore,* $\mathbf{v}_j^{t,\mathbf{p}_0}$, $j = 1, \ldots, d$ *are the Koopman modes of the full-state observable and the following expansion is valid*

$$U^{t,\mathbf{p}_0}\mathbf{x}_0 = \sum_{j=1}^{d} \langle \mathbf{x}_0, \mathbf{w}_j^{t,\mathbf{p}_0} \rangle e^{\lambda_j^{t,\mathbf{p}_0}} \mathbf{v}_j^{t,\mathbf{p}_0}. \tag{47}$$

Data-driven algorithms and Hankel matrix (1)

An observable $f : X \to \mathbb{C}$ of the nonautonomous dynamical system can be reinterpreted as an observable of the skew product flow, i.e., $g : P \times X \to \mathbb{C}$ with the definition

$$g(\mathbf{y}(t, \mathbf{y}_0)) = f(\mathbf{x}(t, \mathbf{p}_0, \mathbf{x}_0)), \tag{48}$$

where $\mathbf{y} = (\mathbf{p}, \mathbf{x}) \in P \times X$. In that sense, propagation in time of such observable can be covered by the nonautonomous Koopman operator (3), but it can also be covered by the autonomous Koopman operator of the skew product flow

$$U^t g = g \circ \mathbf{S}_s^t. \tag{49}$$

Now, let us consider what the data-driven algorithms can give us on the nonautonomous Koopman operator family. If we apply the cocycle property to the time $t = k\Delta t$, then for the autonomous Koopman operator (of the skew product flow) we get

$$U_S^{k\Delta t} = (U_S^{\Delta t})^k. \tag{50}$$

However, if we apply the same in the case of the nonautonomous Koopman operator family in the process formulation we obtain

$$U^{t_0+k\Delta t, t_0} = U^{t_0+k\Delta t, t_0+(k-1)\Delta t} \circ U^{t_0+(k-1)\Delta t, t_0(k-2)k\Delta t} \circ \ldots \circ U^{t_0+\Delta t, t_0}. \tag{51}$$

Similarly, if we apply the same in the case of the nonautonomous Koopman operator family in the skew product formulation we obtain

$$U^{k\Delta t, \mathbf{p}_0} = U^{\Delta t, \theta^{(k-1)\Delta t}(\mathbf{p}_0)} \circ U^{\Delta t, \theta^{(k-2)\Delta t}(\mathbf{p}_0)} \circ \ldots \circ U^{\Delta t, \mathbf{p}_0}. \tag{52}$$

Data-driven algorithms and Hankel matrix (2)

For a chosen vector observable $\mathbf{f} = (f_1, \ldots, f_N)^T : X \to \mathbb{C}^N$ we can form the Hankel matrix $\mathbf{H}$

$$\mathbf{H} = \begin{pmatrix} \mathbf{f}_0 & \mathbf{f}_1 & \cdots & \mathbf{f}_{m_H-1} & \mathbf{f}_{m_H} \\ \mathbf{f}_1 & \mathbf{f}_2 & \cdots & \mathbf{f}_{m_H} & \mathbf{f}_{m_H+1} \\ \vdots & \vdots & \ddots & \vdots & \\ \mathbf{f}_{n_H-1} & \mathbf{f}_{n_H} & \cdots & \mathbf{f}_{n_H+m_H-2} & \mathbf{f}_{n_H+m_H-1} \end{pmatrix}. \tag{53}$$

for $r = 1, \ldots, N, i = 0, \ldots, n_H - 1,\ j = 0, \ldots, m_H$. After that, we can apply the Vandermonde-Cauchy algorithm (Z. Drmač). The Vandermonde-Cauchy algorithm has the data snapshots as the input, and as the output it provides us with a set of Ritz values and vectors

$$(\mu_j, \mathbf{R}_j), j = 1, 2, ..., m_H. \tag{54}$$

Observe that the Ritz vectors are of dimension $n_H \cdot N$, which is the number of rows of the Hankel matrix, and that each Ritz vector is an approximation of the corresponding eigenfunction evaluation at $\mathbf{f}_0$ multiplied with the related Koopman mode of the vector observable. From Ritz values we approximate the Koopman operator eigenvalues λ_j, $j = 1, 2, ..., m_H$

$$e^{\lambda_j \Delta t} = \mu_j, j = 1, 2, ..., m_H. \tag{55}$$

Finally, we use the expression

$$\tilde{\mathbf{f}}(t) = \sum_{j=1}^{m_H} \mu_j^{\frac{t-t_0}{\Delta t}} \mathbf{R}_j \tag{56}$$

Data-driven algorithms and Hankel matrix (3)

as an algorithm-given approximation of the observable. This expression corresponds with the decomposition in Proposition 2 and Proposition 1.
As we already commented, the Hankel matrix can be understood as created by the action of the autonomous Koopman operator (of the skew product flow) on the observable (48)

$$H_{N\cdot i+r,j+1} = U_S^{(i+j)\Delta t} g_r(\mathbf{y}_0) = (U_S^{\Delta t})^{(i+j)} g_r(\mathbf{y}_0). \tag{57}$$

In this interpretation, the result from [1] might be applicable. In particular, if the autonomous skew product flow is ergodic and if observables are in an invariant subspace of the Koopman operator, the eigenvalues and eigenvectors obtained by the DMD algorithm used on the Hankel matrix, converge to the true Koopman eigenvalues and eigenfunctions of the considered system.
On the other hand, if we have the ambition to compute the eigenvalues and eigenfunctions of the nonautonomous Koopman operator family, we can interpret the same Hankel matrix in the process formulation

$$H_{N\cdot i+r,j+1} = U^{t_0+(i+j)\Delta t,t_0} f_r(\mathbf{x}_0), \tag{58}$$

or in the skew product flow formulation

$$H_{N\cdot i+r,j+1} = U^{(i+j)\Delta t,\mathbf{p}_0} f_r(\mathbf{x}_0). \tag{59}$$

Example of an oscillator with the driven amplitude (1)

We consider a nonautonomous differential equation of the form

$$\begin{pmatrix} \dot{x}_1 \\ \dot{x}_2 \end{pmatrix} = \begin{pmatrix} (\sigma_0 + A_d \cos(\omega_d t) + B_d \sin(\omega_d t))x_1 + \omega_0 x_2 \\ -\omega_0 x_1 + (\sigma_0 + A_d \cos(\omega_d t) + B_d \sin(\omega_d t))x_2 \end{pmatrix}. \tag{60}$$

Alternatively, we can set an autonomous differential equation that corresponds to the driving parameter

$$\begin{pmatrix} \dot{p}_1 \\ \dot{p}_2 \end{pmatrix} = \begin{pmatrix} \omega_d p_2 \\ -\omega_d p_1 \end{pmatrix}, \tag{61}$$

and then reformulate (60) into

$$\begin{pmatrix} \dot{x}_1 \\ \dot{x}_2 \end{pmatrix} = \begin{pmatrix} (\sigma_0 + p_1)x_1 + \omega_0 x_2 \\ -\omega_0 x_1 + (\sigma_0 + p_1)x_2 \end{pmatrix} \tag{62}$$

Observe that the process formulation (60) satisfies conditions of the Proposition 1, while the skew product formulation (61)-(62) satisfies conditions of the Proposition 2. We concentrate on just one observable - the first component of the full-state observable, i.e., $f = x_1$. For that observable, we form a Hankel matrix (53, $N = 1$). The time we cover with the snapshot span we present as the Hankel matrix time span $T_H = (n_H + m_H + 1)\Delta t$. In all computations we apply the Vandermonde-Cauchy algorithm ([2, 3]).

Example of an oscillator with the driven amplitude (2)

To investigate different settings of the skew product flow, we perform the computations for different periods of the driving parameter ($T_d = 2\pi/\omega_d$) and of the non-driven oscillator ($T_0 = 2\pi/\omega_0$). In Fig. 7, subfigures (a) and (b) correspond to the intrinsic period larger then the driven $T_0 > T_d$, subfigures (c) and (d) correspond to equal intrinsic and driven period $T_0 = T_d$, while subfigures (e) and (f) correspond to the intrinsic period smaller then the driven period $T_0 < T_d$. Also, all presented computations are performed with $A_d = B_d = 1$, i.e., the initial state of the parameter $\mathbf{p}_0 = (1, 1)$.

Our first goal is to compute the nonautonomous Koopman operator eigenvalues and eigenfunctions. In hope to catch these local eigenvalues and eigenfunctions, we use Hankel matrix with a relatively small snapshot span. The corresponding results are presented in Fig. 7, subfigures (a), (c), and (e).

Our second goal is to see if we can, through that one observable, discover the eigenvalues and eigenfunctions of the related skew product flow which is an autonomous dynamical system. In that case we use Hankel matrix with a large snapshot span (see [1]). The corresponding results are presented in Fig. 7, subfigures (b), (d), and (f).

Example of an oscillator with the driven amplitude (3)

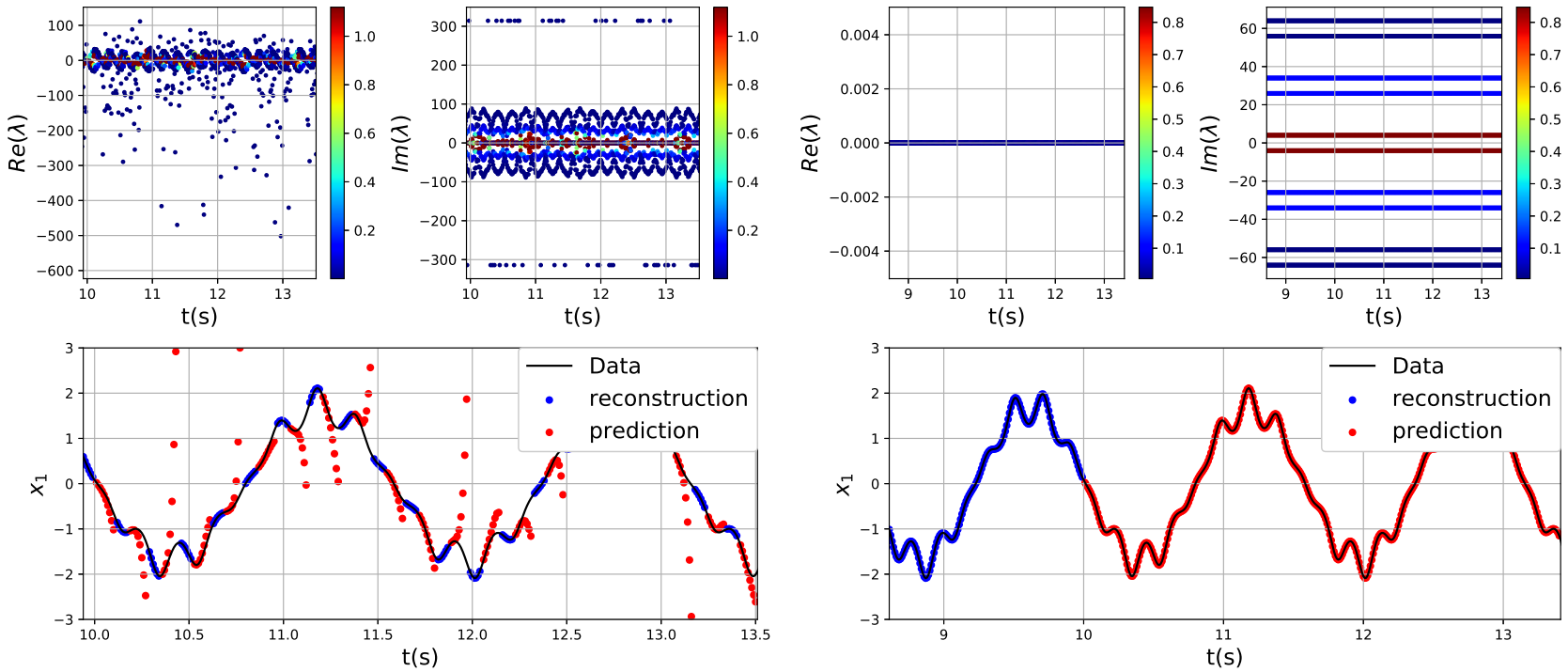

(a) $T_0 = \pi/2,\ T_d = \pi/15,\ T_H = \pi/10$ (b) $T_0 = \pi/2,\ T_d = \pi/15,\ T_H = \pi$

Figure: Oscillator with the driven amplitude: computations obtained with the Vandermonde-Cauchy algorithm on the Hankel matrix for single observable $f = x_1$

Example of an oscillator with the driven amplitude (4)

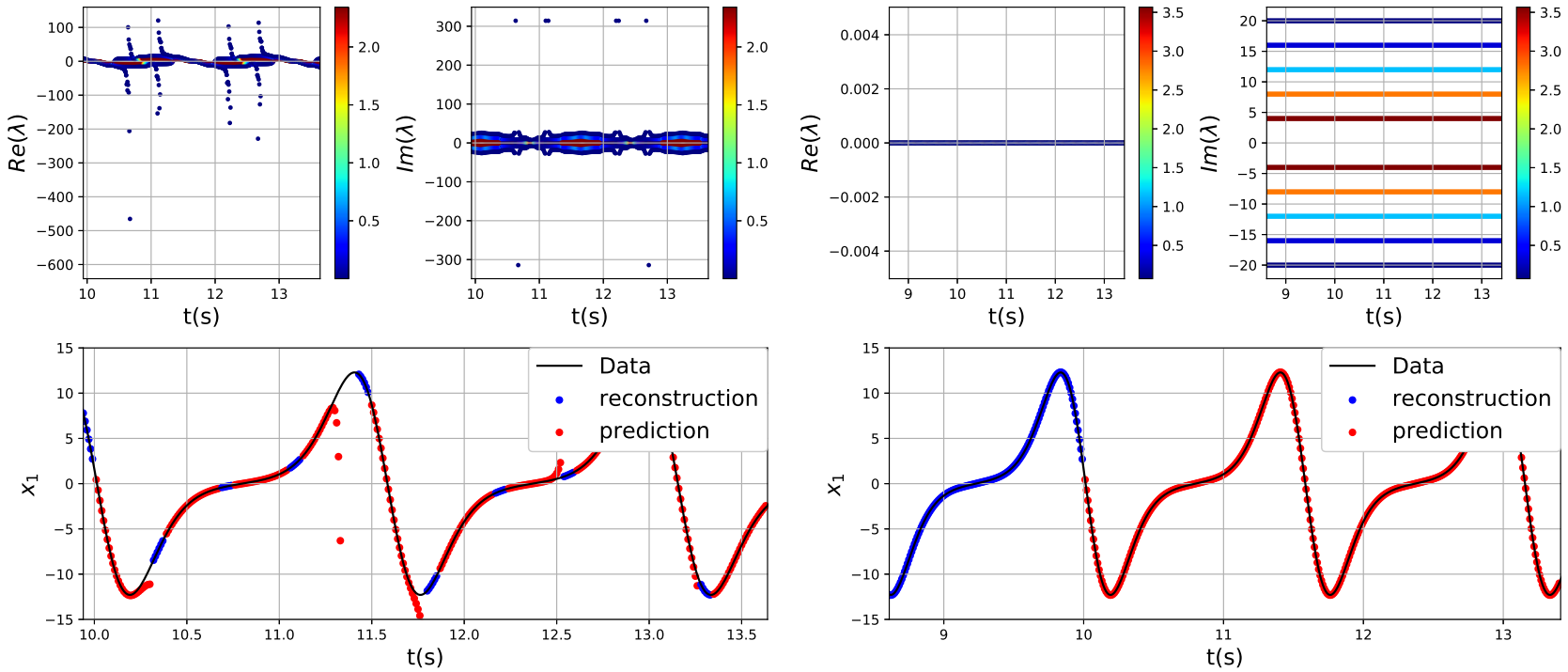

(c) $T_0 = \pi/2,\ T_d = \pi/2,\ T_H = \pi/10$ (d) $T_0 = \pi/2,\ T_d = \pi/2,\ T_H = \pi$

Figure: Oscillator with the driven amplitude: computations obtained with the Vandermonde-Cauchy algorithm on the Hankel matrix for single observable $f = x_1$

Example of an oscillator with the driven amplitude (5)

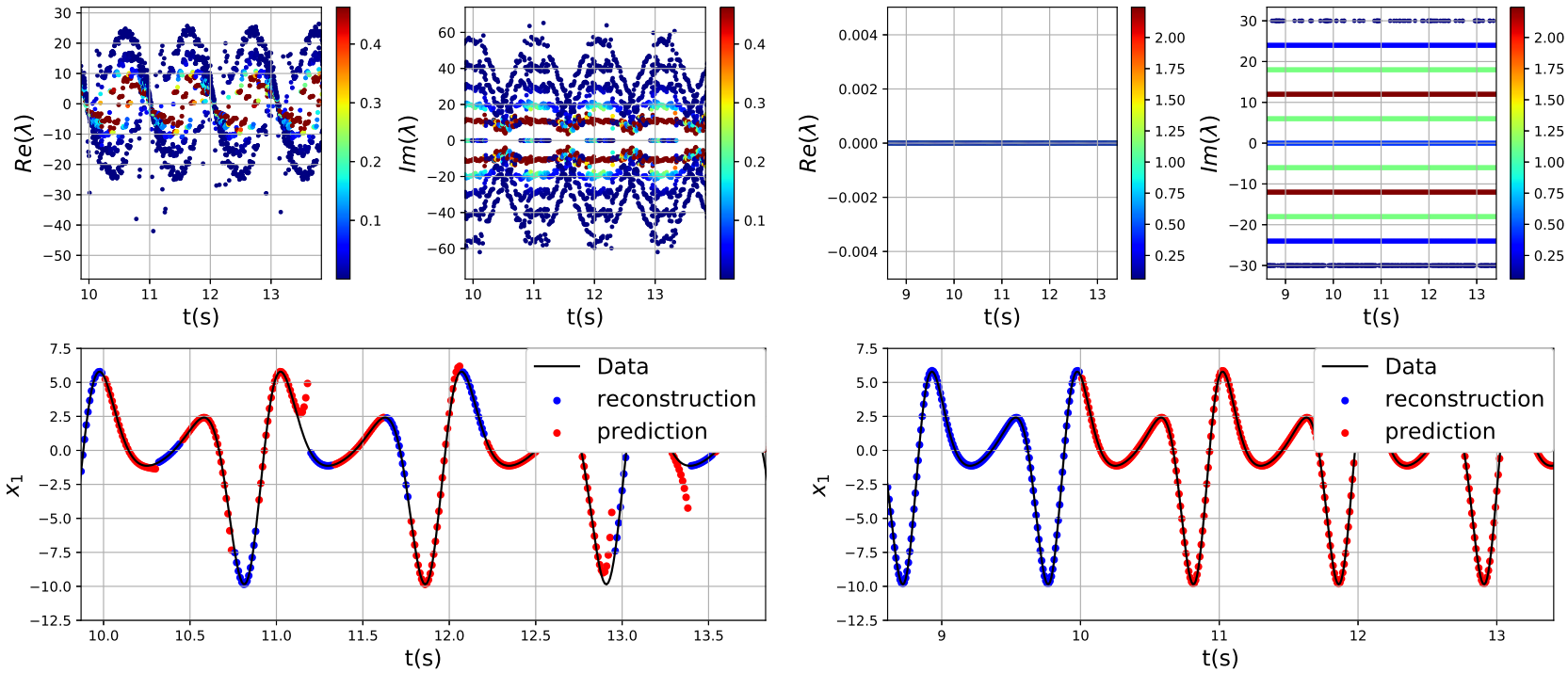

(e) $T_0 = \pi/6,\ T_d = \pi/3,\ T_H = \pi/10$ (f) $T_0 = \pi/6,\ T_d = \pi/3,\ T_H = \pi$

Figure: Oscillator with the driven amplitude: computations obtained with the Vandermonde-Cauchy algorithm on the Hankel matrix for single observable $f = x_1$


Arbabi, H., Mezić, I.: Ergodic theory, Dynamic Mode Decomposition and Computation of Spectral Properties of the Koopman operator, SIAM J. Appl. Dyn. Syst., 16 (2017), pp. 2096-2126


Drmač, Z., Mezić, I., Mohr, R.: Data driven modal decompositions: analysis and enhancements. SIAM J. Sci. Comput., 40(4) (2018), pp. A2253-A2285


Drmač, Z., Mezić, I., Mohr, R.: Data driven Koopman spectral analysis in Vandermonde-Cauchy form via the DFT: numerical method and theoretical insights. ArXiv e-prints, (2018), https://arxiv.org/abs/1808.09557


Maćešić, S., Črnjarić-Žic, N, Mezić, I.: Koopman operator family spectrum for nonauonotomus systems. SIAM J. Appl. Dyn. Syst., 17(4) (2018), pp. 2478-2515